Available online at www.sciencedirect.com
SCIENCE DIRECT®
Journal of Solid State Chemistry 177 (2004) 2943–2950
JOURNAL OF SOLID STATE CHEMISTRY
http://elsevier.com/locate/jssc

Crystal structure and vibrational spectrum of the $NaCaMg_2F_7$ pyrochlore

E.A. Oliveira,[a] I. Guedes,[a] A.P. Ayala,[a,*] J-Y. Gesland,[b] J. Ellena,[c] R.L. Moreira,[d] and M. Grimsditch[e]

[a] *Departamento de Física, Universidade Federal do Ceará, Caixa Postal 6030, 60451-970, Fortaleza, Ceará, Brazil*
[b] *Université du Maine-Cristallogénèse, UMR 6087, 72085 Le Mans Cedex 9, France*
[c] *Instituto de Física de São Carlos-USP, Caixa Postal 369, 13560-970, São Carlos, São Paulo, Brazil*
[d] *Departamento de Física, ICEx, Universidade Federal de Minas Gerais, Caixa Postal 702, 30123-970, Belo Horizonte, Minas Gerais, Brazil*
[e] *Argonne National Laboratory, Materials Science Division, Argonne, IL 60439, USA*

Received 31 January 2004; received in revised form 29 April 2004; accepted 30 April 2004

Abstract

The crystalline structure of $NaCaMg_2F_7$ was determined using single crystal X-ray diffraction. This compound crystallizes in the cubic pyrochlore structure, i.e., space group $Fd\bar{3}m$, lattice parameter: $a = 10.2610(5)$ Å and $Z = 8$. All atoms occupy special crystalline sites, but Na and Ca are randomly distributed in the anti-cristobalite sub-lattice of the pyrochlore structure. The vibrational spectrum was determined by polarized Raman scattering and infrared reflectance. The number of observed Raman and infrared active phonons is larger than that predicted by the factor group analysis of the pyrochlore structure. The anomalous vibrational spectrum is discussed in terms of a disorder-induced symmetry lowering mechanism.

Keywords: Pyrochlore; Vibrational spectrum; Disorder; Symmetry lowering

1. Introduction

Compounds that are isostructural to the mineral pyrochlore $((Na,Ca)_2(Nb,Ta)_2O_6(O,F,OH))$ form a populous family with more than 150 members. All of these compounds have a regular or distorted pyrochlore structure, which has the form $A_2B_2X_6X'$ (where X and $X' = O, F, S, OH$) and can be viewed as two interpenetrated networks, one of BX_6 corner-sharing octahedra and another of A_2X' arranged as an anti-cristobalite sublattice [1]. This structure crystallizes in a face centered cubic lattice belonging to the $Fd\bar{3}m$ space group with eight formulas units per unit cell. When the A_2X' sublattice is replaced by larger monovalent cations (A'), such as Cs^+ or Rb^+, this structure is commonly designated as modified pyrochlore structure ($\square_2B_2X_6A'$, $\square$ is a vacancy). Two large families of compounds are known to crystallize in these structures: oxides, with the formula $A_2^{3+}B_2^{4+}O_7$ (where A/B can be magnetic and A^{4+} is often a rare-earth ion) and fluorides, with the formula $A(M_{1/2}^{2+}M_{1/2}{}'^{3+})_2F_6$ (where A is often an alkali-metal ion, and M^{2+} and M'^{3+} are usually transition-metal ions).

From the structural point of view, the oxide family is well ordered, while in most of the compounds belonging to the fluoride family, the M^{2+} and M'^{3+} ions are randomly distributed in the octahedral sites. However, some compounds, such as $LiFe^{2+}Fe^{3+}F_6$ [2], $NH_4Fe^{2+}Fe^{3+}F_6$ [3,4] and NH_4CoAlF_6 [5], are ordered, but their symmetry is reduced to the space group $P4_2/mnm$ (D_{4h}^{14}). One of the most relevant characteristics of the pyrochlores is related to their magnetic properties, since its structure shows a strong geometric frustration. Evidently, the magnetic properties of these compounds depend strongly on the distribution of the M^{2+} and M'^{3+} ions in octahedral sites. For disordered compounds, such as $CsMnFeF_6$ [6] and $CsNiCrF_6$ [7,8],

*Corresponding author. Fax: +55-85-288-9450.
E-mail address: ayala@fisica.ufc.br (A.P. Ayala).

0022-4596/$ - see front matter © 2004 Elsevier Inc. All rights reserved.
doi:10.1016/j.jssc.2004.04.055

anomalous magnetic behaviors, such as spin glass and spin-ice order, are observed contradicting the high geometrical frustration of the pyrochlore structure [9]. An insight into the consequences of the disordered structure on the inhibition of geometrical frustration of modified pyrochlores was achieved by investigating their vibrational spectra. Recently, the vibrational spectra of the $CsInMgF_6$ modified pyrochlore was investigated by polarized Raman scattering and infrared reflectance spectroscopy [10]. The spectra could not be interpreted in the framework of group theory analysis of the pyrochlore structure. However, by considering the first neighbor coordination polyhedra of each non-equivalent atomic species, it was observed that the disorder suppresses some symmetry operations which transforms the $Fd\bar{3}m$ space group into the $R\bar{3}m$ subgroup. The group theory analysis based on the $R\bar{3}m$ subgroup gave the correct number of observed vibrational bands and also their scattering geometry dependence and relative intensities.

Beside the modified pyrochlore family, another group of fluoride compounds crystallizes in the regular pyrochlore structure. Thus, by distributing randomly monovalent and divalent cations in the A site it is possible to compensate the reduction of the anionic charge due to the complete substitution of X and X' by fluorine. As a consequence the new family has the form $(A^{1+}_{1/2}A_{1/2}{}'^{2+})_2B_2^{2+}F_7$ or, in a more compact form, $A^{1+}A'^{2+}B_2^{2+}F_7$. As far as we know, the only report of a compound of this family was presented by Kubel et al. [11] for $NaSrMg_2F_7$. Using X-ray powder diffraction, they confirmed the pyrochlore structure of this material but were not able to obtain single crystals. In this work we report, for the first time, the single crystal structure determination of the $NaCaMg_2F_7$ pyrochlore. In addition, polarized Raman scattering and infrared reflectivity were used to obtain the vibrational spectrum of this compound. The effects of the A site disorder are discussed on the basis of symmetry reduction.

2. Experimental

$NaCaMg_2F_7$ has a very congruent melting, in about 900°C. Single crystals of $NaCaMg_2F_7$ several cm^3 in size have been pulled from stoichiometric melts using the Czochralski technique. A colorless crystal of dimensions $0.05 \times 0.07 \times 0.10\ mm^3$ was used for structural investigation. X-ray diffraction measurements were made on an Enraf–Nonius Kappa-CCD difractometer with graphite monochromated Mo$K\alpha$ ($\lambda = 0.71073$ Å) radiation. Data were collected up to 60° in 2θ, with a redundancy of 4. The final unit cell parameters were based on the 1439 collected reflections with the following index ranges: $0 \leqslant h \leqslant 13, -13 \leqslant k \leqslant 14, -14 \leqslant l \leqslant 14$. Data collections were made by using the COLLECT program [12]; integration and scaling of the reflections were performed with the HKL Denzo–Scalepack system of programs [13]. Absorption corrections were carried out using the multi-scan method [14]. The structure was solved using Patterson methods with SHELXS-97 [15]. The model was refined by full-matrix least-squares procedures on F^2 using SHELXL-97 [16]. The program WINGX was used to analyze and prepare the data for publication [17]. Crystal data, data collection procedures, structure determination methods and refinement results are summarized in Tables 1–3.

The sample used for Raman and infrared measurements, with dimensions of $3.0 \times 3.0 \times 3.0\ mm^3$ was cut

Table 1
Crystal data and structure refinement

Empirical formula	$NaCaMg_2F_7$
Formula weight	307.76
Crystal system	Cubic
Space group	$Fd\bar{3}m$
Unit cell dimensions	$a = 10.2610(5)$ Å
Volume	1080.39(9) $Å^3$
Z	8
Density (calculated)	3.784 Mg/m^3
Absorption coefficient	2.594 mm^{-1}
$F(000)$	1192
Reflections collected/unique	1439/88 ($R_{int} = 0.1217$)
Data/parameters	88/13
Goodness-of-fit on F^2	1.127
Final R indices [$I > 2\sigma(I)$]	$R_1 = 0.0310$, $wR_2 = 0.0761$
Absolute structure parameter	−0.06(4)
Largest diff. peak and hole	1.607 and −3.666 e.$Å^{-3}$

Table 2
Atomic coordinates ($\times 10^4$), equivalent isotropic displacement parameters ($Å^2 \times 10^3$), occupation factor (f) and anisotropic displacement parameters ($Å^2 \times 10^3$)

	x	y	z	U (eq)	f	U_{11}	U_{22}	U_{33}	U_{23}	U_{13}	U_{12}
Na	5000	5000	5000	58(4)	0.5	58(3)	58(3)	58(3)	0	0	0
Ca	5000	5000	5000	22(4)	0.5	22(1)	22(1)	22(1)	0	0	0
Mg	0	0	0	16(1)	1.0	16(1)	16(1)	16(1)	0(1)	0(1)	0(1)
$F(1)$	3750	3750	3750	22(1)	1.0	22(1)	22(1)	22(1)	0	0	0
$F(2)$	3270(1)	1250	1250	25(1)	1.0	29(1)	24(1)	24(1)	−7(1)	0	0

U(eq) is defined as one-third of the trace of the orthogonalized U_{ij} tensor. The anisotropic displacement factor exponent takes the form $-2\pi^2[h^2a^{*2}U_{11} + \cdots + 2hka^*b^*U_{12}]$.

Table 3
Selected interatomic distances of the $NaCaMg_2F_7$ pyrochlore

Mg–Mg	3.6278(2)
Mg–*F*(2)	1.9788(6)
Mg–*F*(1)	4.2540(2)
(Na,Ca)–(Na,Ca)	3.6278(2)
(Na,Ca)–*F*(1)	2.2215(1)
(Na,Ca)–*F*(2)	2.5375(1)
F(1)–*F*(1)	4.4431(1)
F(1)–*F*(2)	3.0571(1)
F(2)–*F*(2)	2.9323(1)

with faces perpendicular to the [110], [1$\bar{1}$0] and [001] directions and was carefully polished with diamond paste. Raman spectra were recorded using a Jobin–Yvon Triplemate Spectrometer (model T64000) equipped with a LN_2–cooled CCD detector. The spectra were taken in the right angle configuration, using 50 mW of the 476 nm line of a Spectra Physics 170 Krypton ion laser as exciting source. Scattering geometries for the spectra listed in the text and figures follow the usual Porto's notation, $A(BC)D$ [18]. Reflection infrared spectra were recorded with a BOMEM DA8 Fourier Transformer spectrometer, in the range 30–4000 cm^{-1}. The spectral resolution was typically 4 cm^{-1}. For the mid infrared region (above 400 cm^{-1}), the best choice of accessories was: globar source, coated KBr beamsplitter and LN_2–cooled HgCdTe detector. The far infrared region was measured using Globar or Mercury arc lamp (below 200 cm^{-1}), 6 μm coated-mylar Hypersplitter^{TM} and LHe–cooled Si bolometer.

3. Results

3.1. Crystalline structure

Single crystal X-ray diffraction confirms that $NaCaMg_2F_7$ crystallizes in the $Fd\bar{3}m$ (O_h^7) space group with eight molecules per unit cell. The results of the data refinement are summarized in Tables 1 and 2, where the origin was set at the Mg cation (setting II). Notice that in the pyrochlore structure all atoms occupy special positions and just the x coordinate of the $F(2)$ anion is free to change from one compound to other. As it was pointed out by Subramanian et al. [1], the x value determines the coordination of A and B sites. For $x = 0.3125$, B cations are at the center of regular octahedra, while for $x = 0.375$, A cations are at the center of regular cubes. The $NaCaMg_2F_7$ data shows an intermediate value showing that neither the A nor B coordination polyhedra are regular. In this way, the description of the pyrochlore structure as two interpenetrating networks of AX'_2 and BX_6 is not formally correct since this structure does not support octahedral sites. However, as this description is widely used and the obtained x value suggests an almost regular octahedral coordination, it was maintained. Fig. 1 shows the [110] projection of $NaCaMg_2F_7$.

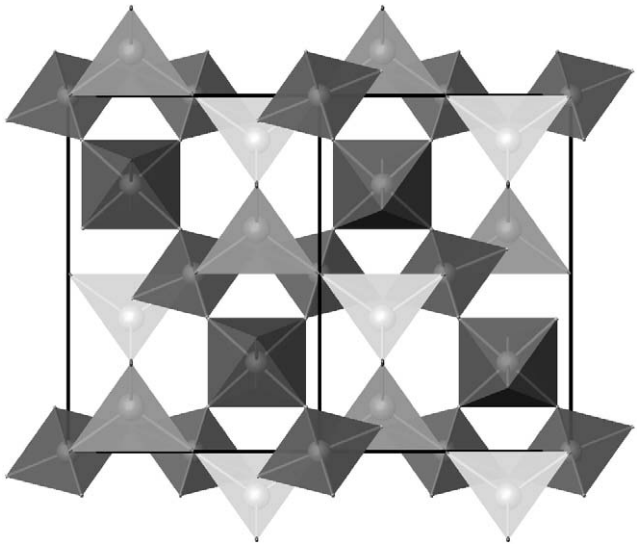

Fig. 1. [110] projection of the $NaCaMg_2F_7$ crystalline structure. Dark polyhedra represent the MgF_6 octahedra with $F(2)$ anion placed in the corners. Light polyhedra stand for $(Na,Ca)_4F$ tetrahedra where $F(1)$ occupy the central site and the cations are in the corners.

Table 3 lists some selected interatomic distances. As it can be observed Mg–$F(2)$ and $F(2)$–$F(2)$ distances, which determine the octahedra, are approximately the sum of the Mg^{2+} (0.7 Å) and F^- (1.3 Å) ionic radii. Thus, we can assume the octahedra are closely packed and ionically bonded. On the other hand, the distorted cube surrounding the A site, which is occupied by Na and Ca, is less compact than the octahedra, but it is also expected to be determined by ionic bonds as it is usual in the pyrochlore family.

3.2. Factor group analysis

According to the X-ray data, the disordered cations (Na and Ca) share 16*d* Wyckoff positions, while Mg cations are in 16*c* ones; both sites have D_{3d} ($\bar{3}m$) symmetry. The fluorine ions occupy 8*b* and 48*f* Wyckoff positions, which have $T_d(\bar{4}3m)$ and $C_{2v}(mm2)$ symmetries, respectively. Based on this information and using the site group analysis proposed by Rousseau et al. [19], it is possible to calculate the irreducible representation at the center of the Brillouin zone (Γ point). The results of the factor group analysis are summarized in Table 4.

By considering the character table of the O_h point group, seven phonons belonging to the F_{1u} representation are infrared active, while six vibrational modes should be observed in Raman spectroscopy. Additional information can be obtained from Raman scattering if one takes advantage of the symmetry dependence of the polarizability tensors ($\tilde{\alpha}$). Thus, by using polarized

Table 4
Factor group analysis of the $NaCaMg_2F_7$ crystal structure

Ion	Wyckoff site	Symmetry	Irreducible representations
Na/Ca	16*d*	D_{3d}	$A_{2u}\oplus E_u\oplus 2F_{1u}\oplus F_{2u}$
Mg	16*c*	D_{3d}	$A_{2u}\oplus E_u\oplus 2F_{1u}\oplus F_{2u}$
F(1)	8*b*	T_d	$F_{1u}\oplus F_{2g}$
F(2)	48*f*	C_{2v}	$A_{1g}\oplus A_{2u}\oplus E_g\oplus E_u\oplus 2F_{1g}\oplus 3F_{1u}\oplus 3F_{2g}\oplus 2F_{2u}$
Total	$\Gamma = A_{1g}\oplus 3A_{2u}\oplus 3E_u\oplus E_g\oplus 8F_{1u}\oplus 2F_{1g}\oplus 4F_{2u}\oplus 4F_{2g}$		
Acoustic	$\Gamma_{ac} = F_{1u}$		
Raman	$\Gamma_R = A_{1g}\oplus E_g\oplus 4F_{2g}$		
Infrared	$\Gamma_{IR} = 7F_{1u}$		

Table 5
Intensity of the Raman active vibrational modes in different scattering geometries

Configuration	A_{1g}	E_g	F_{2g}
zz	a^2	$4b^2$	0
$x'y'$	0	$3b^2$	0
$y'z$	0	0	$d^2/2$

radiation, the Raman intensity can be written as

$$I \propto |\mathbf{e}_o^{\dagger}\cdot\tilde{\alpha}\cdot\mathbf{e}_i|^2, \quad (1)$$

where $\mathbf{e_i}$ and $\mathbf{e_o}$ are the polarization vectors of the incoming and outgoing radiation, respectively. The $\tilde{\alpha}$ tensors corresponding to the Raman active representations of the O_h point group are [20]

$$A_{1g}: \begin{pmatrix} a & . & . \\ . & a & . \\ . & . & a \end{pmatrix},$$

$$E_g: \begin{pmatrix} b & . & . \\ . & b & . \\ . & . & -2b \end{pmatrix}, \quad \begin{pmatrix} -\sqrt{3}b & . & . \\ . & \sqrt{3}b & . \\ . & . & . \end{pmatrix}, \quad (2)$$

$$F_{2g}: \begin{pmatrix} . & . & . \\ . & . & d \\ . & d & . \end{pmatrix}, \quad \begin{pmatrix} . & . & d \\ . & . & . \\ d & . & . \end{pmatrix}, \quad \begin{pmatrix} . & d & . \\ d & . & . \\ . & . & . \end{pmatrix}.$$

The Raman intensities calculated from (1) and (2) in different scattering geometries are listed in Table 5, where, in addition to the crystallographic axes, two other polarization directions are considered : x' ([110]) and y' ([1$\bar{1}$0]). Notice that in the *zz* configuration both A_{1g} end E_g modes should be observed, whereas in the $y'z$ geometry just the F_{2g} modes are active. In order to separate A_{1g} from E_g modes the $x'y'$ scattering geometry can be used since only E_g modes are allowed in it. This methodology has been successfully used in other cubic system to obtain its complete vibrational spectrum [21].

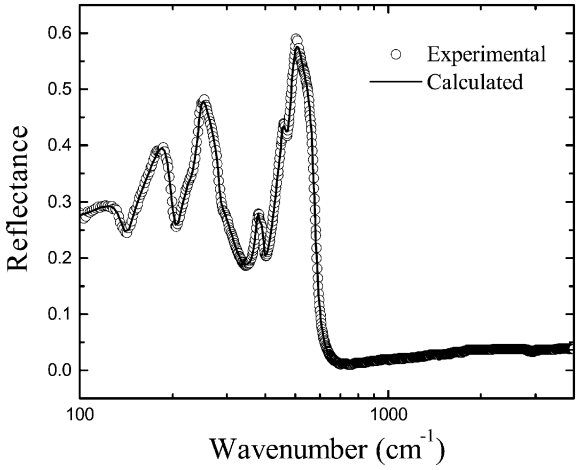

Fig. 2. Reflectance spectrum of $NaCaMg_2F_7$. Open circles and solid lines stand for experimental and calculated spectra, respectively.

3.3. Infrared reflectance spectroscopy

The infrared dielectric function was determined by carrying out a dispersion analysis of the observed spectra on the basis of the four parameter semi-quantum model [22,23]. According to this model, the complex dielectric constant is expressed in terms of the infrared active modes as follows:

$$\epsilon(\omega) = \epsilon_\infty \prod_j \frac{\omega_{jLO}^2 - \omega^2 + i\omega\gamma_{jLO}}{\omega_{jTO}^2 - \omega^2 + i\omega\gamma_{jTO}}, \quad (3)$$

where ω_{jTO} and ω_{jLO} correspond to the resonance frequencies of the *j*th transverse and longitudinal modes, respectively, and γ_{jTO} and γ_{jLO} are the corresponding damping factors. ϵ_∞ is the dielectric constant due to the electronic polarization. The observed infrared reflectivity **R** is fitted with the aid of Eq. (3), together with [24]

$$\mathbf{R} = \left|\frac{\sqrt{\epsilon}-1}{\sqrt{\epsilon}+1}\right|^2. \quad (4)$$

The reflectivity spectrum of $NaCaMg_2F_7$ is shown in Fig. 2. The calculated spectrum using the method outlined above fits very well to the corresponding

Table 6
Dielectric dispersion parameters of the $NaCaMg_2F_7$ obtained from the best fit to the experimental data

ω_{TO}	γ_{TO}	ω_{LO}	γ_{LO}	$\Delta\varepsilon_{TO}$
138	25	140	17	0.349
188	33	201	20	2.277
225	53	239	25	2.171
244	17	285	16	0.682
286	19	325	142	0.007
379	14	382	13	0.065
387	14	390	20	0.034
437	43	446	32	0.402
450	27	470	41	0.167
482	35	555	122	0.197
559	75	582	44	0.006
	$\varepsilon_\infty = 2.18$		$\varepsilon_0 = 8.54$	

Frequencies and dampings are in cm^{-1}.

experimental one. Table 6 lists the parameters of longitudinal and transversal modes, used to obtain the best fit to the reflectivity curves.

We noticed that, although the Gervais's et al. semi-quantum model [22,23] reproduces very well the measured spectra, 11 vibrational bands were required to obtain a good fit of the experimental data, whereas the factor group analysis of the cubic $NaCaMg_2F_7$ structure predicts only seven infrared active modes. Such an anomalous feature has often been observed in disordered materials. The most usual consequences of the atomic disorder are the so-called one-phonon [25,26] and two-phonon [27,28] behavior. In the first case the frequencies of some vibrational modes, those corresponding to the disordered species, vary proportionally to the reduced mass of the disordered atoms, preserving the number of infrared active bands. This is not the case here because the number of observed vibrational modes has increased. In the second model (two-phonon behavior), some bands split due to the mass difference of the disorder atoms. This hypotheses is ruled out here because disordered induced band splitting should be expected only in the infrared spectra (see Table 4) with addition of, at most, two modes, increasing the number of active bands to nine instead of the eleven bands observed. Recently, Ayala et al. [10] showed, in a modified pyrochlore crystal, the increase of the observed bands could be explained by considering a symmetry reduction model. The $NaCaMg_2F_7$ infrared spectrum will be discussed later on the basis of this mechanism.

3.4. Raman scattering

According to the factor group analysis, Raman spectra recorded in $z(x'y')x'$, $z(y'z)x'$ and $x'(zz)y'$ scattering geometries should be enough to identify the complete set of optical active phonons. Indeed the following irreducible representations should be observed in these scattering geometries (see Tables 4 and 5):

$$x'(zz)y'\text{: } A_{1g} \text{ and } E_g,$$
$$z(x'y')x'\text{: } E_g,$$
$$z(y'z)x'\text{: } 4F_{2g}. \quad (5)$$

Raman spectra recorded in these scattering geometries are shown in Fig. 3a. All spectra are characterized by wide bands between 50 and 500 cm^{-1}. Notice that two phonon modes are expected in the $x'(zz)y'$ spectrum, and just one in the $z(x'y')x'$ one. However, a larger number of bands are detected in these geometries. By using a computer-based software to fit the recorded data to a set of damped harmonic oscillators, we identified 8, 10 and 8 bands in the $z(x'y')x'$, $z(y'z)x'$ and $x'(zz)y'$ spectra, respectively. The wavenumbers of the identified bands are listed in Table 7. As in the case of the infrared spectrum the number of vibrational bands observed in the Raman spectra is larger than that predicted by the factor group analysis. Furthermore, the spectra recorded in the $z(x'y')x'$ and $x'(zz)y'$ scattering geometries are similar; only slight differences are observed in the first and second wide bands. On the other, in the $z(y'z)x'$ spectrum, the low-energy bands are more intense suggesting they would have a F_{2g}-like behavior. However, the occupational disorder induced increase of the Raman active bands precludes any attempt to classify the bands on the basis of the irreducible representations of the O_h point group. The origin of such an anomalous

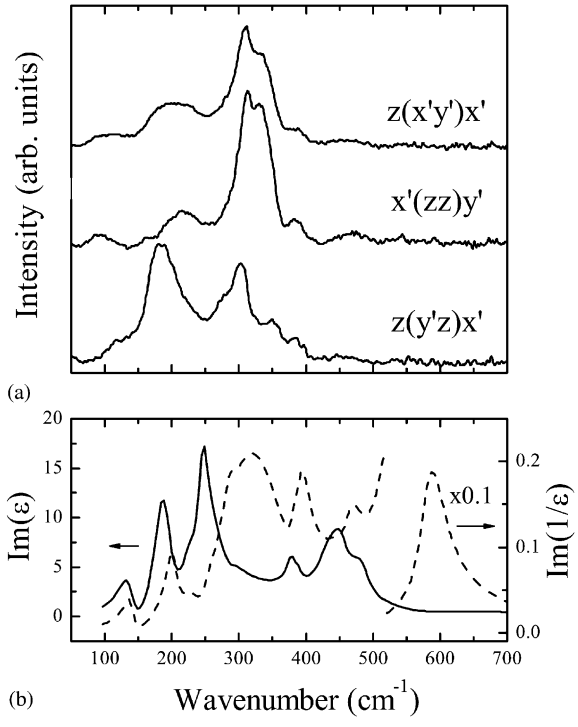

Fig. 3. (a) Raman spectra of $NaCaMg_2F_7$ recorded in different scattering geometries. (b) Optical functions calculated from the infrared reflectance spectra.

Table 7
Raman active vibrational modes (in cm^{-1}) observed in different scattering geometries

$x'(zz)y'$	$z(x'y')x'$	$z(y'z)x'$
91	88	
	117	126
161	176	179
202	203	211
224	229	
	275	275
311	308	303
338	338	350
385	385	386
469	458	453

behavior, and its correlation with the infrared reflectance results will be discussed in the next section.

4. Discussion

By comparing, our structural and vibrational results it is possible to notice an apparent contradiction. While the X-ray diffraction analysis yields a well-defined crystalline structure, the vibrational spectrum does not agree with the factor group prediction based on this structure. The origin of these discrepancies comes from the differences in the scope of each technique. Thus, X-ray diffraction gives an average structure, whereas the vibrational techniques depict the local balance among the interatomic forces.

In order to gain an insight into the mechanism that induces the anomalous vibrational spectra of the $NaCaMg_2F_7$ pyrochlore, we compared the phonon spectra observed by Raman scattering and infrared reflectance. This comparison is best achieved by using the optical functions derived from the four-parameters semi-quantum model [22,23]. Thus, the frequencies of the maxima in the imaginary part of the complex dielectric constant (ε'') roughly correspond to the frequencies of transverse optical phonons. Furthermore, it is well known that the imaginary part of the reciprocal dielectric constant (η'') peaks at the frequencies of the longitudinal optical modes [23]. These optical functions were plotted in Fig. 3b. Although, Raman and infrared bands originate from different mechanisms, and their intensities cannot be compared directly, it is still possible to notice the strong similarities between both experimental results. Indeed, in the present case, almost all infrared-active vibrational bands can be directly associated to a Raman-active one. The only exceptions are the low-energy Raman bands, which are outside the spectral range recorded in the infrared measurements, and the strong higher energy infrared band. The last one should be associated to the anti-symmetric stretching of the MgF_6 octahedra, which is usually weak or forbidden in Raman spectra. Based on these results, we infer that the main effect of the random occupation of the A-site is to relax the vibrational selection rules, allowing Raman active phonons to be observed in the infrared spectrum and vice versa. Thus, the $NaCaMg_2F_7$ pyrochlore has a non-centrosymmetric-like vibrational spectra.

Occupational disorder induced symmetry lowering has been recently observed in the $CsInMgF_6$ modified pyrochlore [10]. In this system, a careful analysis of the first-neighbors showed that the fluorine site symmetry is reduced due to the random distribution of the cation at the octahedra center. Due to this fact, the fluorine site symmetry is reduced from C_{2v} to C_s removing the C_4 axes of the pyrochlore structure and transforming the $Fd\bar{3}m$ space group into the $R\bar{3}m$ subgroup. As a consequence of this symmetry lowering mechanism, the neighboring octahedra of the BX_6 network become non-equivalent and the vibrational spectrum behaves like that of a rhombohedral system.

In the case of the $NaCaMg_2F_7$ pyrochlore, the disordered cations lie in the anti-cristobalite network, where F_1 anions are surrounded by the randomly occupied A sites, which form a regular tetrahedron around the anion. It is difficult to define a single mechanism of symmetry reduction because different distributions of Na and Ca in the F_1 neighborhood induce different subgroups of the $Fd\bar{3}m$ space group. However, some evidence of a symmetry lowering based on the F_1 sites can be found from the apparent loss of the inversion center. Notice that F_1 anions are placed at sites with T_d symmetry, which is a non-centrosymmetric point group. In fact, the inversion center located at the A site connects two neighbor tetrahedra (see Fig. 4).

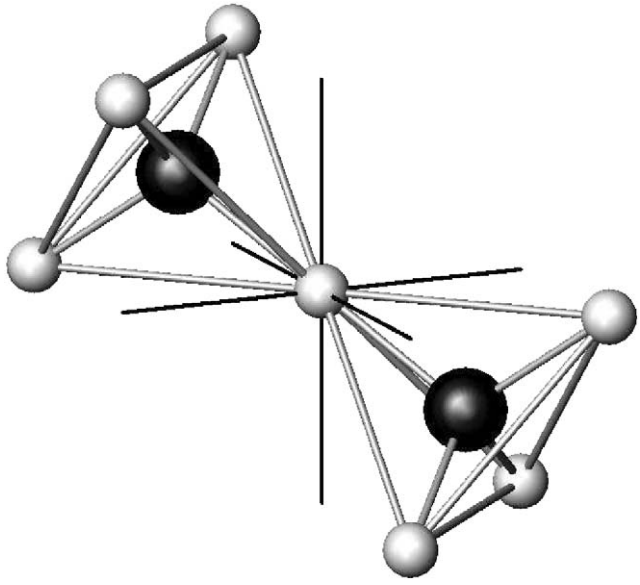

Fig. 4. Coordination polyhedra of the $F(1)$ anions. Light and dark spheres stand for $F(1)$ and A atoms. Thin lines represent the crystallographic axes.

Such a symmetry lowering induces a mechanism similar to that observed in the modified pyrochlores, that is, neighboring polyhedra of the disordered network are no longer equivalent. By considering the maximal subgroup of the $Fd\bar{3}m$ space group resulting from the suppression of the inversion center, the crystal symmetry should be reduced to the $F\bar{4}3m$ (T_d^2), which preserves the orientation and size of the crystalline axes, as well as the tetrahedral coordination of the F_1 sites. Calculating the new irreducible representation, we obtain

$$\Gamma = 4A_1 + 4E + 6F_1 + 12F_2, \tag{6}$$

where the Raman active representations are A_1, E and F_2, while F_1 is silent and F_2 is also infrared-active. One of the F_2 representations corresponds to the acoustic phonons. As a consequence, the following representations are expected to be Raman and infrared active:

$$\Gamma_{\mathrm{R}} = 4A_1 + 4E + 11F_2,$$
$$\Gamma_{\mathrm{IR}} = 11F_2. \tag{7}$$

Due to the correlation between the point group O_h and its subgroup T_d, the increase in the number of the totally symmetric (A_1) and doubly degenerated (E) Raman active modes comes from the silent modes of the O_h point group $(A_{2u} \rightarrow A_1,\ E_u \rightarrow E)$. Furthermore, the 11 F_2 modes result from the combination of the $4F_{2g}$ with $7F_{1u}$. Notice the remarkable agreement of the number of bands predicted by the symmetry lowered structure with the experimental results. First, the number of predicted infrared active phonons agrees with the observed one. Moreover, most of these bands are also observed in the $z(y'z)x'$ Raman spectrum, which agrees with the F_{2g} and F_{1g} mixture into the new F_2 representation. The only exception is the high energy band of the infrared spectra, which, however, is expected to be very weak in Raman spectroscopy, as already pointed out. Conversely, the F_2-type band at around 300 cm^{-1} is faint in the infrared reflectance spectrum.

Even though the crystallographic axes are preserved in the lower symmetry structure and T_d and O_h point groups have the same Raman scattering tensors (see Eq. (2)), our results do not show the suppression of the A_1 phonons in the $z(x'y')x'$ scattering geometry. Indeed, the spectrum for this configuration is rather similar to that of the totally symmetric $x'(zz)y'$, i.e., they should both correspond to the mixture $4A_1 + E$. Finally, the bands around 320 cm^{-1} should be associated to the symmetric stretching of the fluoride octahedra, which belongs to the A_1 representation. This vibrational mode should be infrared forbidden and Raman-active. By observing the reflectance spectra we can see that it has a low reflectivity in the region around this wavenumber region.

5. Conclusions

Single crystal X-ray diffraction, infrared reflectance and Raman scattering have been used to investigate the crystalline structure and the vibrational spectrum of $NaCaMg_2F_7$. Our results confirm the pyrochlore structure with Na^+ and Ca^{2+} cations randomly distributed in the A site. Polarized Raman and infrared spectra show a larger number of vibrational bands than that predicted by factor group analysis. The most remarkable result is the apparent loss of the inversion center, evidenced by the relaxation of the Raman and infrared selection rules. Assuming a non-centrosymmetric subgroup of the pyrochlore structure, we show that the vibrational spectra can be well described on the basis of the $F\bar{4}3m$ space group. This result suggests the symmetry lowering mechanism keeps the tetrahedral symmetry of the F_1 fluorine sites. By comparing our results with those obtained in a modified pyrochlore [10], we propose that the symmetry lowering mechanism in the pyrochlore family originates from the loss of the equivalence of neighboring polyhedra in the disordered network. If the BX_6 sublattice is disordered, the crystal reduces its symmetry to the D_{3d} point group. On the other hand, in the case of the A_2X' sublattice disorder, the loss of the inversion center induces a T_d point group.

Acknowledgments

This work was partially supported by the Brazilian government agencies (CNPq, FAPEMIG and FUNCAP). Work at ANL supported by DOE-BES under Contract W-31-109-ENG38.

References

[1] M.A. Subramanian, G. Aravamudan, G.V. Subbaa Rao, Prog. Solid State Chem. 15 (1983) 55.
[2] N.N. Greenwood, A.T. Howe, F. Menil, J. Chem. Soc. A 13 (1971) 2218.
[3] A. Tressaud, R. de Pape, J. Portier, C.R. Acad. Sci. C. Chim. 270 (1970) 726.
[4] G. Ferey, M. Leblanc, R. de Pape, J. Solid State Chem. 40 (1981) 1.
[5] M.A. Subramanian, W.J. Marshall, R.L. Harlow, Mater. Res. Bull. 31 (1996) 585.
[6] J. Villain, Z. Phys. B 33 (1979) 31.
[7] T. Zeiske, M.J. Harris, M.P. Zinkin, Physica B 234 (1997) 766.
[8] M.P. Zinkin, M.J. Harris, T. Zeiske, Phys. Rev. B 56 (1997) 11786.
[9] M.J. Harris, M.P. Zinkin, Mod. Phys. Lett. B 10 (1996) 417.
[10] A.P. Ayala, C.W.A. Paschoal, I. Guedes, W. Paraguassu, P.T.C. Freire, J. Mendes Filho, R.L. Moreira, J.Y. Gesland, Phys. Rev. B 66 (2002) 214105.
[11] F. Kubel, B. Dundjerski, Z. Anorg. Allg. Chem. 627 (2001) 1589.
[12] Enraf-Nonius, Collect, Nonius BV, Delft, The Netherlands, 1997–2000.

[13] Z. Otwinowski, W. Minor, HKL Denzo and Scalepack, in: C.W. Carter Jr., R.M. Sweet (Eds.), Methods in Enzymology, Vol. 276, Academic Press, New York, 1997, pp. 307–326.
[14] R.H. Blessing, Acta Crystallogr. A 51 (1995) 33.
[15] G.M. Sheldrick, SHELXS-97. Program for Crystal Structure Resolution, University of Gttingen, Gttingen, Germany, 1997.
[16] G.M. Sheldrick, SHELXL-97. Program for Crystal Structures Analysis, University of Gttingen, Gttingen, Germany, 1997.
[17] L.J. Farrugia, ORTEP3 for Windows, J. Appl. Cryst. 30 (1997) 565.
[18] S.P.S. Porto, J.F. Scott, Phys. Rev. B 157 (1967) 716.
[19] D.L. Rousseau, R.P. Bauman, S.P.S. Porto, J. Raman Spectrosc. 10 (1981) 253.
[20] W. Hayes, R. Loudon, Scattering of Light by Crystals, Wiley Interscience, New York, 1978.
[21] M.A.C. Machado, C.W.A. Paschoal, J. Mendes Filho, A.P. Ayala, R.L. Moreira, J.Y. Gesland, J. Phys. Condens. Matter 14 (2002) 271.
[22] F. Gervais, B. Pirou, J. Phys. Condens. Matter 7 (1974) 2374.
[23] F. Gervais, High-temperature infrared reflectivity spectroscopy by scanning interferometry, in: K.J. Button (Ed.), Infrared and Millimetre Waves, Vol. 8, Academic Press, New York, 1983.
[24] D.D. Meneses, desouza@cnrs-orleans.fr, IRFit2.0 adjustment program, Orleans University, France, 1999.
[25] P. Daniel, J. Toulouse, M. Rousseau, Eur. Phys. J. Appl. Phys. 5 (1999) 33.
[26] S.G. Yu, K.W. Kim, L. Bergman, M. Dutta, M.A. Stroscio, J.M. Zavada, Phys. Rev. B 58 (1998) 15283.
[27] R. Mouras, M.D. Fontana, P. Bourson, A.V. Postnikov, J. Phys. Condens. Matter 12 (2000) 5053.
[28] R.L. Moreira, F.M. Matinaga, A. Dias, Appl. Phys. Lett. 78 (2001) 428.